La0.7Sr0.3MnO3 Thin Films for Magnetic and Temperature Sensors at Room Temperature

Sheng Wu, Dalal Fadil, Shuang Liu, Ammar Aryan, B. Renault, Jean-Marc Routoure, Bruno Guillet, Stéphane Flament, Pierre Langlois, Laurence Méchin

$La_{0.7}Sr_{0.3}MnO_3$ Thin Films for Magnetic and Temperature Sensors at Room Temperature

Sheng Wu, Dalal Fadil, Shuang Liu, Ammar Aryan, Benoit Renault, Jean-Marc Routoure, Bruno Guillet, Stéphane Flament, Pierre Langlois and Laurence Méchin

Université de Caen Basse-Normandie, UMR 6072 GREYC, F-14032 Caen, France
ENSICAEN, UMR 6072 GREYC, F-14050 Caen, France
CNRS, UMR 6072 GREYC, F-14032 Caen, France
E-mail: laurence.mechin@ensicaen.fr

Abstract: In this paper, the potentialities of the manganese oxide $La_{0.7}Sr_{0.3}MnO_3$ (LSMO) for the realization of sensitive room temperature thermometers and magnetic sensors are discussed. LSMO exhibits both a large change of the resistance versus temperature at its metal-to-insulator transition (about 330 K) and low field magnetoresistive effects at room temperature. The sensor performances are described in terms of signal-to-noise ratio in the 1 Hz - 100 kHz frequency range. It is shown that due to the very low 1/f noise level, LSMO based sensors can exhibit competitive performances at room temperature.

Keywords: Low frequency noise, Magnetoresistance sensors, Thermometers.

---

1. Introduction

Due to the colossal magnetoresistance effect and the strong spin polarization at the Fermi level, the rare earth manganese oxides may find important applications in magnetoresistive devices such as magnetic random access memories and magnetic sensors [1, 2]. In addition, the large change of their electrical resistance R at the metal-to-insulator transition, which takes place in the 300 - 350 K range makes them potential materials for the fabrication of room temperature thermometers. Ideal materials would indeed present at the desired operating temperature T close to 300 K:

i) a high temperature coefficient of the resistance (β_T), expressed in K^{-1} and defined as the relative derivative of the resistance versus temperature $\beta_T = (1/R) \times (dR/dT)$, or a high relative change of the resistance with the magnetic field (β_H), expressed in T^{-1}, and defined as $\beta_H = (1/R) \times (dR/d(\mu_0 H))$ (with μ_0 the vacuum permeability), and
ii) a low noise level.

The limits of the device performances are given by the signal-to-noise ratio.

Temperature coefficient of the resistance values and operating temperatures are important parameters to be considered in the fabrication of high sensitivity room-temperature thermometers or magnetoresistances. However, more attention should be paid to the low-frequency noise level in these materials since it can vary by several orders of magnitude while β_H or β_T values may only vary by a factor less than 10. However noise is more difficult to optimize since its origin is still not well known [3-8]. To reduce noise, high material quality is required and a large number of measurements are needed in order to determine the general trend for the evolution of noise with geometrical parameters such as width, length, and sample thickness.

Even if it does not exhibit the highest β_H or β_T values, $La_{0.7}Sr_{0.3}MnO_3$ (LSMO) has been selected among all the possible manganite compositions because it has shown the lowest reported low-frequency noise level so far [8-10].

In this paper, details about sample preparation are presented in section 2. In section 3, the low frequency noise measurement set-up is presented. A discussion about the sensor performances as a function of the geometry, of the bias condition and of the frequency is given in section 4. The performances of LSMO based thermometers as well as magnetoresistive sensors are finally presented and compared with published values.

2. Sample Preparation

The sensors are patterned in 100 nm thick LSMO thin films deposited by pulsed laser deposition from a stoichiometric target onto $SrTiO_3$ (001) single crystal substrate. The laser radiation energy density, the target-to-substrate distance, the oxygen pressure and the substrate temperature were 220 mJ, 50 mm, 0.35 mTorr and 720 °C, respectively.

The deposition conditions were found optimal for producing single-crystalline films as judged by X-ray diffraction. The X-ray diffraction study indicated a full (001) orientation of the LSMO films as shown by the θ–2θ scan of Fig. 1. Full Width at Half Maximum measured in a ω-scan configuration around the LSMO 002 peak was 0.2°.

An Atomic Force microscopy (AFM) study was performed in tapping mode. As shown in Fig. 2, we observed very smooth surface (with rms roughness of 0.2 nm) and terraces at the film surface.

Electrical resistivity and saturated magnetization were measured in the unpatterned film. They are reported in Fig. 3. Both resistivity and saturated magnetization values are close to those measured in bulk LSMO, thus confirming the overall good quality of the tested sample.

After LSMO deposition, a 200 nm thick gold layer was sputtered on the films in order to make low resistive connections. The LSMO thin films were patterned by UV photolithography and argon ion etching to form lines. As shown in Fig. 4, the mask enables the study of lines of four different widths W = 20, 50, 100 and 150 μm. For each width, five lengths L could be measured depending on the

position of the voltage contacts L = 50, 100, 150, 200, and 300 μm. Tens of samples with different geometries have been investigated. In this paper, we chose to report typical results for 50 μm wide 300 μm long line patterned in a 100 nm thick LSMO film.

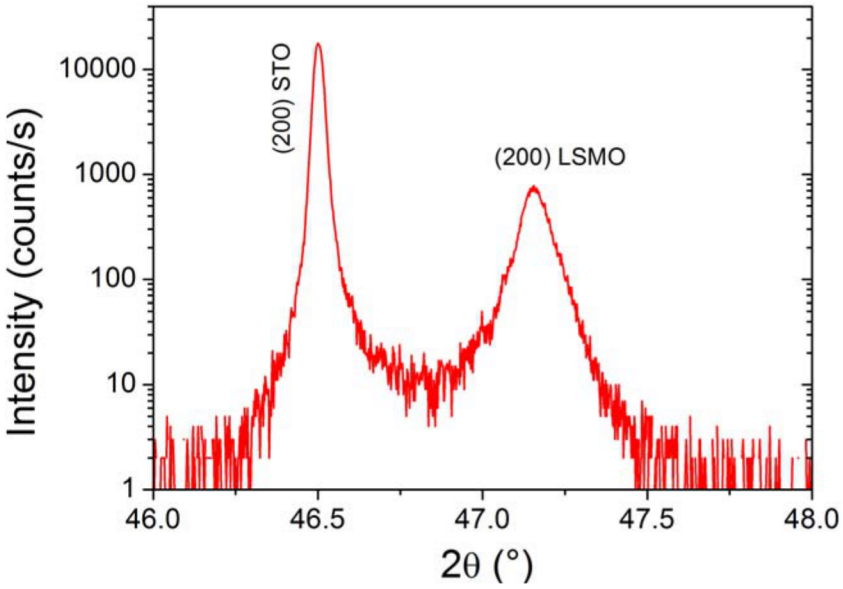

Fig. 1. X-ray diffraction pattern in the θ–2θ configuration of the 100 nm thick LSMO films on STO(001).

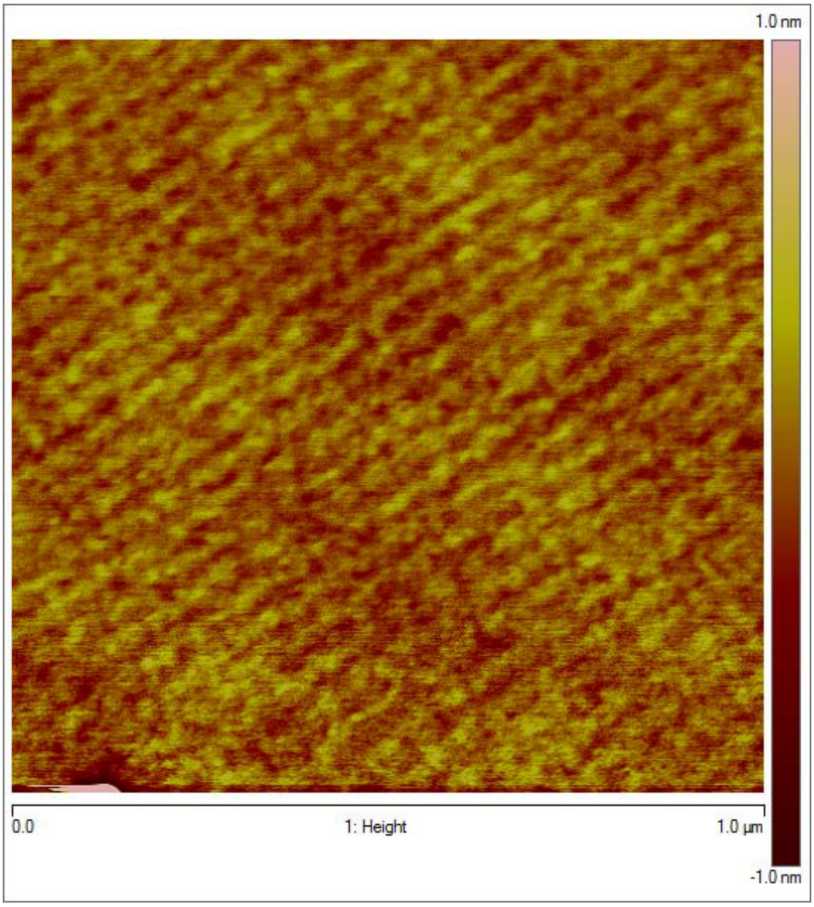

Fig. 2. 1 μm × 1 μm AFM image in tapping mode of the 100 nm thick LSMO film on STO (001).

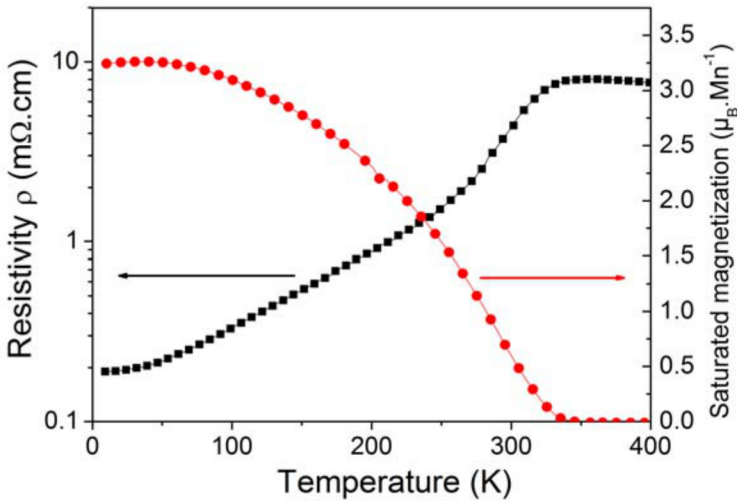

Fig. 3. Electrical resistivity (left axis – black squares) and saturated magnetization in 500 Oe (right axis – red circles) versus temperature of the 100 nm thick LSMO film deposited on STO (001).

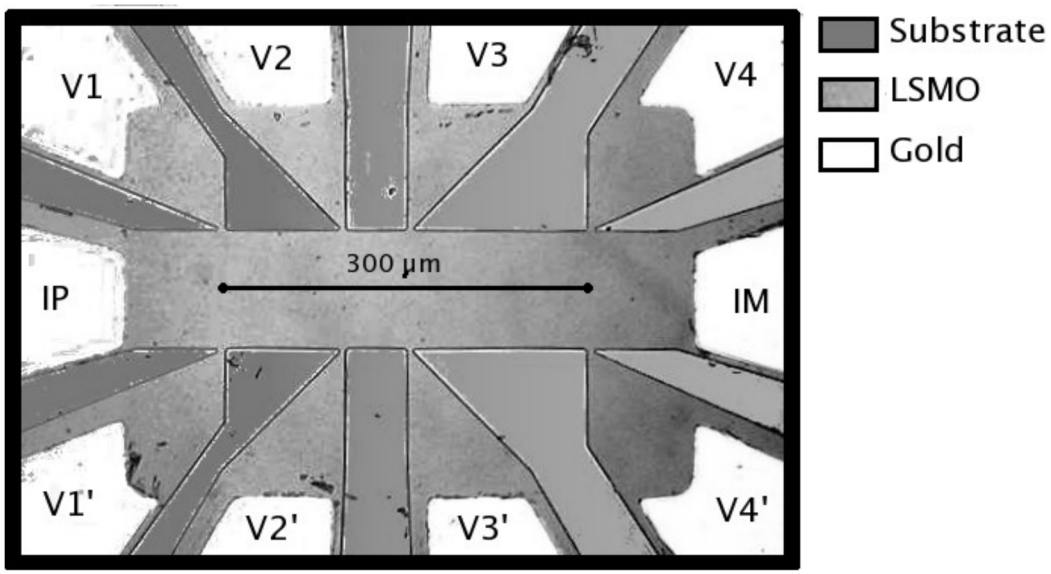

Fig. 4. Optical photography of a 100 μm width line with the two current probes IP and IM and 4 voltage probes (V1...V4, V1'...V4') on each side of the line. The line lengths between V1 -V2, V2 - V3 and V3 -V4 are 100 μm, 50 μm and 150 μm, respectively.

3. Low Frequency Noise Measurements

3.1. Measurement Set-up and Protocol

The experimental set-up mainly consists in one low noise high output impedance DC current source and a dedicated low noise instrumentation amplifier with the following characteristics: a DC output dedicated to resistance measurement with a voltage gain equal to 10 and an AC output dedicated to noise measurements with a voltage gain around one thousand and a 1 Hz - 1 MHz bandwidth [11]. The input voltage white noise is around 20×10^{-18} $V^2 \cdot Hz^{-1}$ and its input current noise is negligible. The device is connected at the output of the DC current source using IP and IM pads (defined in Figs. 4 and 5). The DC voltage as well as the voltage noise are measured using the instrumentation amplifier connected either on IP, IM pads for two probe configuration or on Vi, Vj (i,j=1..4 with i≠j) for four

probe configuration. A spectrum analyzer Agilent 89410A calculates the noise spectral density for frequencies in the 1 Hz - 1 MHz range.

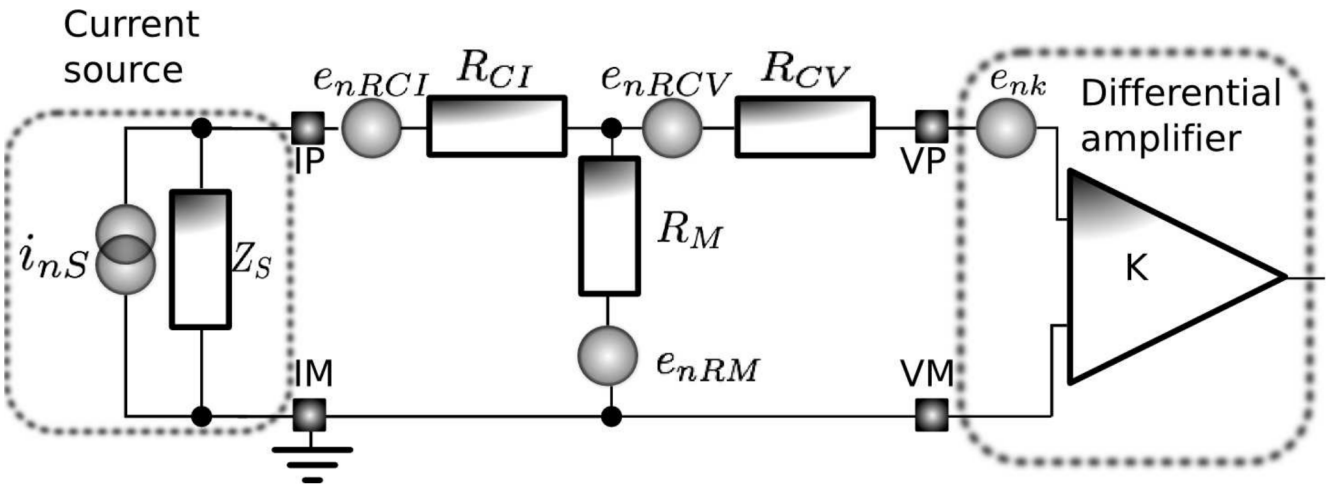

Fig. 5. Schematic representation of the noise measurement set-up showing the four probe technique. The noise sources are located for the current source, the sample and the differential amplifier. Z_S is the output impedance of the current source, R_{CI} is the current contact resistance (for simplicity, R_{CI} is the sum of then current contact resistance of the two probes I_P and I_M), R_M is the film resistance, R_{CV} is the voltage contact resistance (R_{CV} is the sum of the voltage contact resistance of the two probes V_P and V_M), i_{nS} is the current source noise, e_{nRCI} is the current contact resistance noise, e_{nRM} is the film noise, e_{nRCV} is the voltage contact resistance noise and e_{nk} is the differential amplifier noise of spectral density.

According to [11], the DC current source is quasi-ideal, i.e. its output impedance is infinite and its noise contribution is negligible. It is also assumed that the input impedance of the instrumentation amplifier is very high so that no DC current flows in its inputs. It will be also considered that the noise contribution of the amplifier is known and can be subtracted from the measured noise when a device is connected at its input. The noise of the measurement set-up is deduced from the measurement performed at zero bias. This set-up contribution is then removed from all the measured data with applied bias current.

Fig. 6 shows the noise spectral density measured in the two probes (S_{V2p}) and the four probe configurations (S_{V4p}) for the same DC current I. Two noise contributions were found: a white noise one and a 1/f noise one. The white noise level is clearly due the thermal noise contribution given by $4k_BTR$ (k_B is the Boltzmann constant equal to 1.38×10^{-23} $J \cdot K^{-1}$) and should not depend on the bias current. The white noise level is consistent with the expected value deduced from the DC measurement of the sample resistance thus validating the thermal origin of the white noise. One should notice that thermal noise of the voltage contact should have to be taken into account but for simplicity, this contribution as well as the amplifier noise will be neglected in the following: optimal sensor geometries (especially for the voltage contact) and optimized read-out electronic may easily be used to fulfil this requirement indeed.

Different noise contributions that both generate white noise and 1/f noise have to be considered in the sensor: the voltage contact noise, the current contact noise and the film noise (as shown in Fig. 5). Details can be found in [12]. It can be shown that in the two probe configuration, both film and current contact noise contributions are measured. In the four probe configuration, due to the high output impedance of the DC current source, the current contact noise contribution can be completely eliminated. Since no DC current flows into the voltage contact, one would assume that no 1/f noise exists for the voltage contact sources. As shown in Fig. 6, in the four probe configuration (i.e. when

the amplifier is connected to the VP, VM pads), the measured spectral density S_{V4P} is the sample noise spectral density without any correction whereas in the two probe configuration (when the amplifier is connecter to the IP and IM pads), the measured spectral density S_{V2P} is the sum of the current contact noise and the sample noise spectral densities.

The contact contribution originates from the contact between gold and LSMO and thus presents a great impact for sensor applications. Fig. 6 also shows that for this sample, the current contact contribution is much higher than the film noise. This result has already been reported by other studies [13]. It can lead to an overestimation of the film noise if the current source used for the measurement does not exhibit large output impedance.

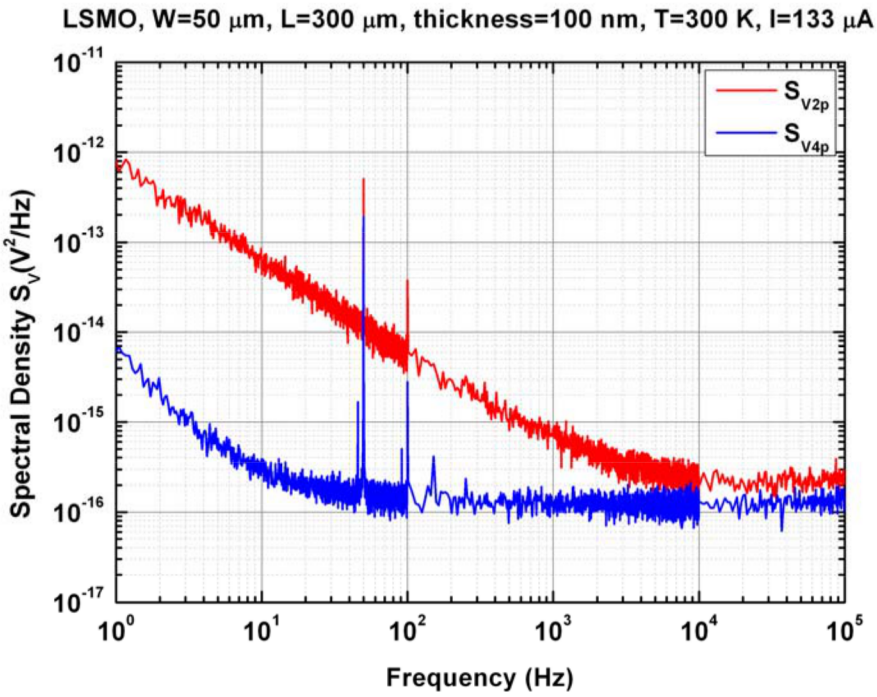

Fig. 6. Noise spectral densities in the two probes (S_{V2p}) and the four probe (S_{V4p}) configurations for the same DC bias current. Using the mask shown in Fig. 4, the current contact noise is non negligible and may have a great impact on sensor performances in the two probe configuration was used.

3.2. Results

Preliminary results presented in Fig. 6 showed that the sensor can not be used in a two contact configuration. A four probe configuration must be used to ensure best signal to noise ratio. Moreover, the metallic pads used for the voltage contacts have also to be placed in a correct manner in order to avoid any possible current path through this metallic contact. As a consequence, metallic voltage pads should not be placed onto the line (like in Transmission Line Measurement (TLM) patterns for instance) but on the side of the line in order to achieve a low frequency noise level sensor.

In these conditions, Fig. 7 shows the voltage noise spectral density measured for a typical device (W=50 μm and L=300 μm) in four probe configuration for different values of the bias current I in the device. As expected, the white noise level does not depend on the bias current but the 1/f noise increases with bias current.

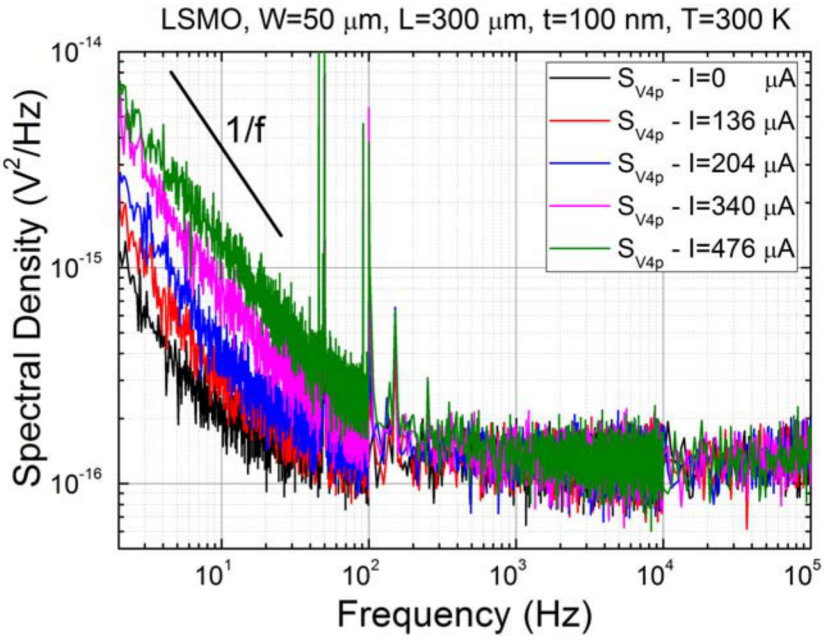

Fig. 7. Noise spectral density measured in the four probe configuration at different bias currents. White noise does not depend on the bias point on the contrary to 1/f noise.

Following the geometrical behaviour reported in homogeneous sample, the 1/f noise level at 1 Hz is in the inverse ratio of the device volume W × L × t [14]. A deviation from this relation can be explained by non homogeneous sample. Finally, the noise spectral density of the sample in the four probe configuration $S_{V4p}(f)$ can be written as follow:

$$S_{V4P}(f) = \frac{K_{1/f}}{f \times W \times L \times t} \times V^2 + \frac{4 \times k_B \times T \times \rho \times L}{W \times t}, \quad (1)$$

where ρ is the film electrical resistivity (typical value is in the 2-4 mΩ·cm for LSMO at 300 K) and $K_{1/f}$ is a material characteristic independent of the geometry that quantify the value of the $K_{1/f}$ noise level. In this sample, $K_{1/f}$ is found around 1×10^{-30} m^3. As reported in [8], this $K_{1/f}$ value is among the lowest reported values for LSMO samples and is comparable with values reported for integrated silicon resistances.

Fig. 8 shows the noise spectral density at 1 Hz versus the sample voltage. In this log-log graph a slope equal to 2 was found, as expected from equation (1) for a quadratic dependence of the noise spectral density S_{V4P} with the sample voltage V. This verified quadratic dependence is an indication that the sample and the noise sources are homogeneous. Equation (1) also clearly shows that length and bias dependency of the noise are completely different in the low frequency and white noise ranges. These discussions will be extended in the next section in the framework of sensor performance analysis.

4. Sensor Performances

In this section, the performances in terms of signal-to-noise ratio will be presented and discussed in the case of thermometers and magnetoresistance sensors.

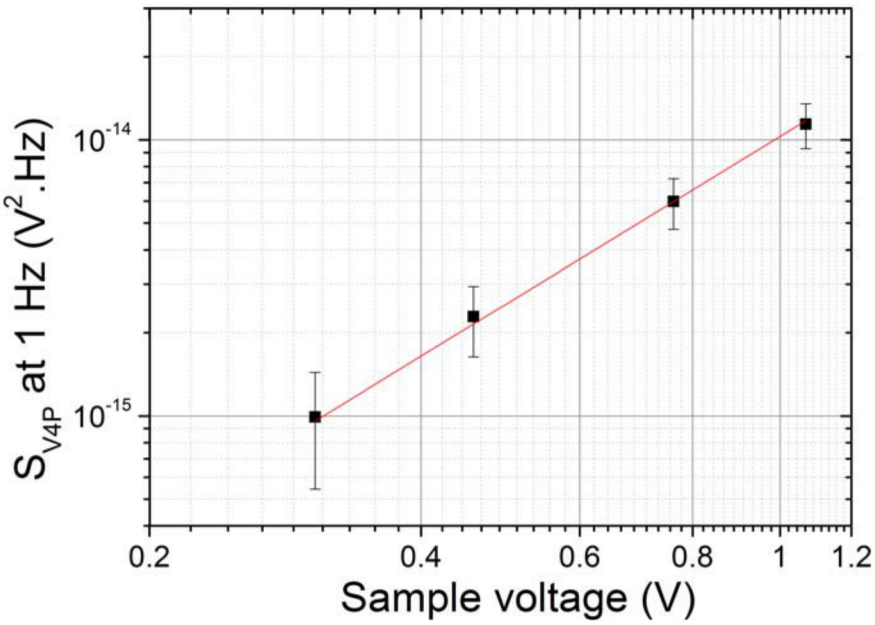

Fig. 8. Noise spectral density at 1 Hz versus the sample voltage.

4.1. Background

To use the devices as sensors, a current source is connected and the voltage across the sensor is measured. A four probe configuration will be used to avoid the current contact noise contribution. Either the temperature T or the magnetic field $\mu_0 H$ are the measurand. For these theoretical derivations, the measurand will be noted M and the relative sensitivity β_M, defined in the following equation, will be used:

$$\beta_M = \frac{1}{R} \times \left(\frac{dR}{dM} \right)_{M0}, \tag{2}$$

where M_0 is the DC value of the measurand for which the relative sensitivity is estimated. The equivalent input sensor noise $S_M(f)$ is given by the ratio of the voltage noise spectral density of the sensor $S_V(f)$ (given by $S_{V4p}(f)$ in the case of our LSMO samples in the previous sample) over the square of the voltage sensitivity at M_0 given by ($dV/dM = V \times \beta_M$). Using equation (1), it follows that $S_M(f)$ finally writes:

$$S_M(f) = \frac{S_V(f)}{(dV/dM)^2} = \frac{1}{\beta_M^2} \left(\frac{K_{1/f}}{f \times W \times L \times t} + \frac{4 \times k_B \times T \times \rho \times L}{V^2 \times t \times W} \right) \tag{3}$$

In order to obtain the smallest noise sensor, this equation shows that in addition to large sensitivity values, low value of the 1/f noise parameter $K_{1/f}$ and low value of the electrical resistivity are first required. Two geometrical and bias dependencies can then be distinguished:

- in the low frequency part where 1/f noise dominates, the equivalent input sensor noise does not depend on the bias and the sample should have the largest volume W × L × t;
- in the white noise range of frequencies, the equivalent input sensor noise decreases with the square of the bias voltage. The geometry should have the smallest ratio value L/W and the sensor should also be as thick as possible.

All these considerations obviously do not take into account other constraints such as frequency bandwidth or cost, which usually leads to opposite conclusions in term of device volume or size. The above noise analysis is illustrated in the next sections for LSMO thermometers and LSMO magnetoresistance sensors (L=300 µm, W=150 µm) considering 1/f noise.

4.2. Thermometers

LSMO electrical resistivity ρ and relative temperature sensitivity β_T (also called TCR for Temperature Coefficient of the Resistance) in case of thermometers versus temperature T are shown in Fig. 9. In this kind of material, a transition from metallic to insulator behaviour occurs for temperature close to room temperature as already reported [15]. In this sample, the maximum value of β_T is found for temperature close to 330 K, and is reported in Table 1.

Table 1. Typical electrical characteristics and noise properties of the film used for the estimation of the signal-to-noise ratio. The values are given for a device length and width of 300 µm and 50 µm, respectively.

Parameter	Value
$K_{1/f}$ (m^3) at 300 K	1×10^{-30}
ρ (Ω· m) at 300 K and at 330 K	3.5×10^{-5} (300K), 6.3×10^{-5} (330K)
β_{TMAX} at 330 K (K^{-1})	2.7×10^{-2}
β_{HMAX} at 300 K (T^{-1})	~ 1

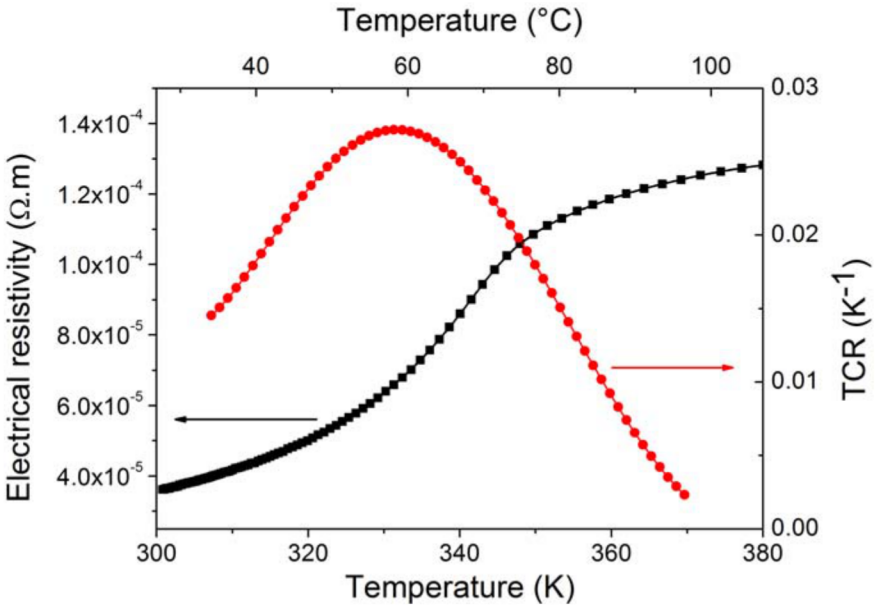

Fig. 9. LSMO electrical resistivity ρ (square symbols, left axis) and relative temperature sensitivity β_T (circle symbols, right axis) versus temperature T in the 300-380 K range for a line with W=50 µm and L=300 µm. The maximum sensitivity is found around 330 K where $\beta_T = 2.7 \times 10^{-2}$ K^{-1}.

4.3. Magnetoresistance Sensors

LSMO electrical resistance and relative magnetic field sensitivity β_H as a function of the magnetic field $\mu_0 H$ are shown in Fig. 10. Due to the ferromagnetic behaviour of LSMO at room temperature, a magnetoresistance effect is observed. Two kinds of effect can be distinguished:

i) a Colossal MagnetoResistance effect (CMR) for magnetic field values greater than 2 mT [16-18], and ii) a low field magnetoresistance effect for magnetic field values close to 0.5 mT.

The first one leads to a small sensitivity with no interesting sensor applications. The second one is related to the magnetization reversal [18-20]. It gives two peaks in the R versus $\mu_0 H$ characteristic and a relatively high value of the relative magnetic field sensitivity (absolute typical values around 1 T^{-1} for an operation point around 1 mT) at room temperature (Table 1).

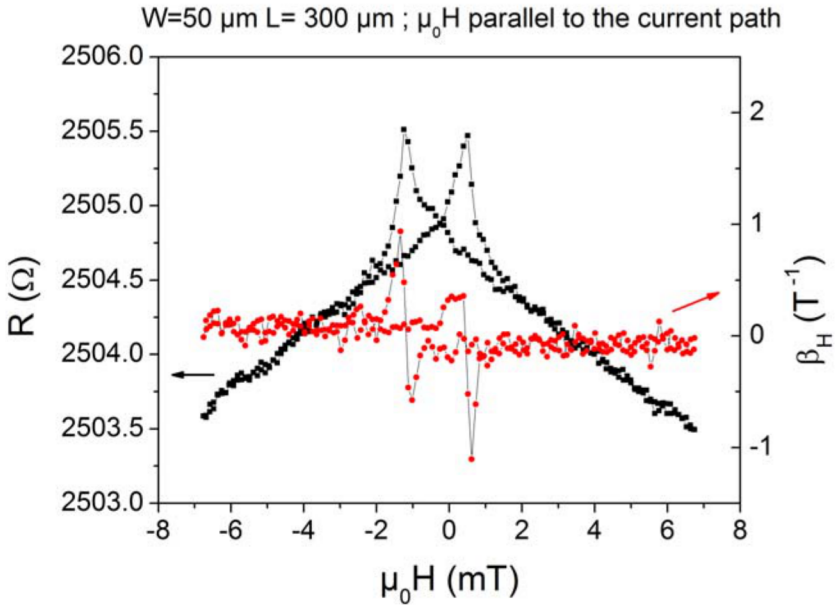

Fig. 10. LSMO electrical resistance R (square symbols, left axis) and relative magnetic field sensitivity β_H (circle symbols, right axis) as a function of the magnetic field $\mu_0 H$ at room temperature for a line with W=50 µm and L=300 µm. Magnetic field is parallel to the current direction. Sensitivity maxima observed at low magnetic field are related to the magnetization reversal in the film.

4.4. Discussion

In this discussion, it will be assumed that the thermometer or the magnetoresistance is connected in four probe configuration and that the device geometry leads to the smallest value of 1/f noise. The noise performances in terms of equivalent input sensor noise values of DC current will be calculated with the data in Table 2 for three values of the DC current I = 100 µA, I = 1 mA and I = 5 mA.

Table 2 summarizes the results for a 150 µm wide and 300 µm long thermometer or magnetoresistance at optimal operating point (330 K for the thermometer, 300 K and 0.1 mT for the magnetoresistance). In this table, the equivalent input sensor noise has been calculated at two frequencies (30 Hz and 10 kHz) to distinguish between the low frequency domain where 1/f noise dominates and the white noise domain.

The equivalent input sensor spectral densities $S_T(f)$ (also called NET for Noise Equivalent Temperature) and $S_H(f)$ calculated using equation 3 and data from table 1 are shown in Fig. 11. As expected, the spectral density at low frequency does not depend on the bias when 1/f noise dominates. On the contrary, at high frequency, the noise level is directly related to the applied bias current. From this figure, it appears that ultimate performances can be achieved at highest current. This remark has obviously to be moderated by the fact that self heating effects occur for too high current values so that the noise performances will be discussed in the following for a bias current limited to 100 µA. At low

bias current, the 1/f noise contribution is negligible. In this LSMO sample, due to the low value of the 1/f noise level, the noise spectral density mainly consists in white noise even at a bias current of about 300 µA.

Table 2. Sensor performances for a 150 µm wide 300 µm long line at different bias current I. (*) R = 700 Ω at 300 K, (**) R = 1260 Ω at 330 K).

Bias current I (mA)	0.1	1	5
$\frac{dV}{d(\mu_0 H)}$ at 300 K (mV/T) (*)	45.5	455	2275
$\sqrt{S_H(f)}$ at 300 K (nT·Hz$^{-0.5}$)			
f = 30 Hz	78	8.6	4.4
f = 10 kHz	75	7.5	1
$\frac{dV}{dT}$ at 330 K (mV/K) (**)	3.4	34	170
$\sqrt{S_T(f)}$ at 330 K (nK·Hz$^{-0.5}$)			
f = 30 Hz	1400	170	100
f = 10 kHz	1400	140	30

The reported NET values are lower (at least one magnitude order) than the one of other uncooled thermometers such as amorphous semiconductors, vanadium oxides, etc. or the well-known Pt100 thermometer [8, 9]. This can easily be explained by the lower noise level of epitaxial manganites thin films compared to others. The results show that despite a quite small TCR value and thanks to a very low-noise level, LSMO thin films are real potential material for uncooled thermometry, as concluded previously by Lisauskas et al. for another manganite composition, namely $La_{0.7}(Pb_{1-x}Sr_x)_{0.3}MnO_3$ [21].

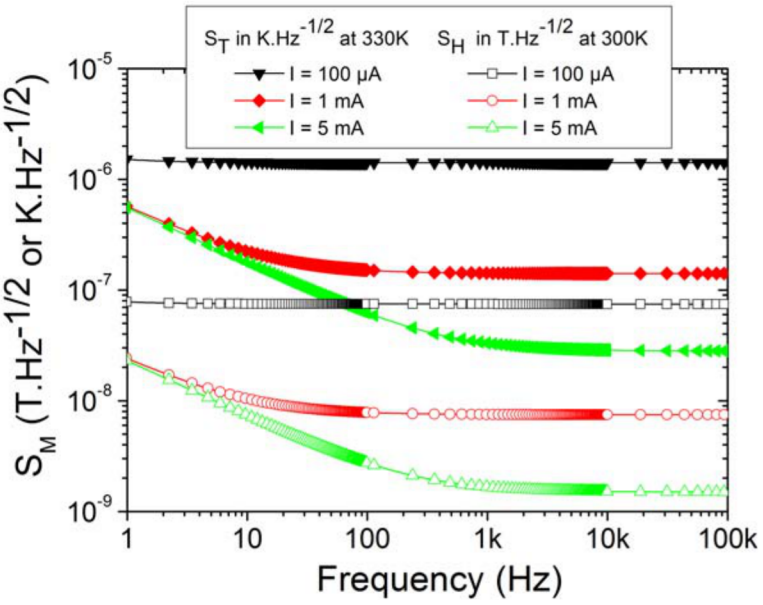

Fig. 11. Square root of the estimated equivalent input sensor spectral densities $S_T(f)$ (filled symbols) or $S_H(f)$ (open symbols) using equation (3) and the table 1 data for three values of the DC current I for a 150 µm width and 300 µm length sensor.

According to [22] where equivalent input sensor spectral densities $S_H(f)$ have been compared for various kinds of magnetic sensors, this LSMO magnetoresistance noise performances are better than Hall effect sensors. Equivalent input sensor spectral densities are only one order of magnitude higher than commercial Honeywell HMC1001 sensors [22-24]. These results are promising since the mask used was not optimized for sensor applications so that the sensitivity could be increased by changing the substrate type or the line geometry. Moreover, it has been demonstrated that LSMO can be deposited onto silicon substrate [25] without modifications of the magnetic properties: compatibility with the standard semiconductor used in the microelectronic industry has thus been demonstrated. This is another way to extend to "More than Moore" idea proposed by the International Roadmap for Semiconductor by the integration of manganese oxide.

5. Conclusion

In this paper, the potentialities of LSMO thin films as magnetic and temperature sensors at room temperature have been reported. It has been shown that a four probe configuration is required to remove the current contact noise that is often several orders of magnitude higher than the material noise. In such conditions, the performances of the room thermometers are in the state of the art for thermometers and that magnetoresistance exhibits noise performances one decade better than classical hall effect sensors.

Acknowledgements

The authors would like to thank C. Fur, J. Gasnier and S. Lebargy for technical assistance in sample fabrication and DC electrical transport measurements.

References

[1]. T. Venkatesan, M. Rajeswari, Z. -W. Dong, S. B. Ogale, and R. Ramesh, Manganite-based devices: opportunities, bottlenecks and challenges, *Philos. Trans. R. Soc. London, Ser. A*, Vol. 356, No. 1742, 1998, pp. 1661–1680.

[2]. M. Bibes, A. Barthélémy, Oxide spintronics, *IEEE Transactions on Electron Devices*, Vol. 54, No. 5, 2007, pp. 1003-1023.

[3]. M. Rajeswari, A. Goyal, A. Raychaudhuri, M. Robson, G. Xiong, C. Kwon, R. Ramesh, R. Greene, T. Venkatesan, and S. Lakeou, 1/f electrical noise in epitaxial thin films of the manganite oxides $La_{0.67}Ca_{0.33}MnO_3$ and $Pr_{0.67}Sr_{0.33}MnO_3$, *Appl. Phys. Lett.,* Vol. 69, No. 6, 1996, pp. 851–853.

[4]. B. Raquet, J. Coey, S. Wirth, and S. von Molnar, 1/f noise in the half-metallic oxides CrO_2, Fe_3O_4, and $La_{2/3}Sr_{1/3}MnO_3$, *Phys. Rev. B*, Vol. 59, No. 19, 1999, pp. 12435–12443.

[5]. A. Lisauskas, S. Khartsev, and A. Grishin, Studies of 1/f Noise in $La_{1-x}Sr_xMnO_3$ (M= Sr,Pb) Epitaxial Thin Films, *J. Low Temp. Phys.,* Vol. 117, No. 5, 1999, pp. 1647–1651.

[6]. A. Palanisami, R. Merithew, M. Weissman, M. Warusawithana, F. Hess, and J. Eckstein, Small conductance fluctuations in a second-order colossal magnetoresistive transition, *Phys. Rev. B*, Vol. 66, No. 9, 2002, p. 92407.

[7]. K. Han, Q. Huang, P. Ong, and C. Ong, Low-frequency noise in $La_{0.7}Sr_{0.3}Mn_{1-x}FeO_3$ thin films, *J. Phys. Condens. Matter*, Vol. 14, 2002, p. 6619.

[8]. L. Méchin, J.-M. Routoure, S. Mercone, F. Yang, S. Flament, and R. Chakalov, 1/f noise in patterned $La_{0.7}Sr_{0.3}MnO_3$ thin films in the 300–400 K range, *J. Appl. Phys*, Vol. 103, 2008, p. 083709.

[9]. F. Yang, L. Méchin, J.-M. Routoure, B. Guillet, and R. A. Chakalov, Low-noise $La_{0.7}Sr_{0.3}MnO_3$ thermometers for uncooled bolometric applications, *J. Appl. Phys*, Vol. 99, No. 2, 2006, p. 024903.

[10]. L. Méchin, J.-M. Routoure, B. Guillet, F. Yang, S. Flament, D. Robbes, and R. Chakalov, Uncooled bolometer response of a low noise $La_{2/3}Sr_{1/3}MnO_3$thin film, *Appl. Phys. Lett.,* Vol. 87, 2005, p. 204103.

[11]. J.-M. Routoure, D. Fadil, S. Flament, and L. M´echin, A low-noise high output impedance DC current

source, in *Proceedings of the 19th International Conference on Noise and Fluctuations (ICNF' 2007), AIP Conference Proceedings*, Vol. 922, No. 1, 2007, pp. 419–424.
[12].C. Barone, A. Galdi, S. Pagano, O. Quaranta, L. Méchin, J. Routoure, and P. Perna, Experimental technique for reducing contact and background noise in voltage spectral density measurements, *Rev. Sci. Instrum.,* Vol. 78, 2007, p. 093905.
[13].C. Barone, S. Pagano, L. Méchin, J.-M. Routoure, P. Orgiani, and L. Maritato, Apparent volume dependence of 1/ f noise in thin film structures: Role of contacts, *Rev. Sci. Instrum.,* Vol. 79, 2008, p. 053908.
[14].F. N. Hooge, 1/f noise is no surface effect, *Phys. Lett.,* 29, A, 3, 1969, p. 139.
[15].A. Urushibara, Y. Moritomo, T. Arima, A. Asamitsu, G. Kido, and Y. Tokura, Insulator-metal transition and giant magnetoresistance in $La_{1-x}Sr_xMnO_3$, *Phys. Rev. B*, Vol. 51, No. 20, 1995, pp. 14103–14109.
[16].J. O'Donnell, M. Onellion, M. Rzchowski, J. Eckstein, and I. Bozovic, Low-field magnetoresistance in tetragonal $La_{1-x}Ca_xMnO_3$ sfilms, *Phys. Rev. B*, Vol. 55, No. 9, 1997, p. 5873.
[17].J. O'Donnell, M. Onellion, M. Rzchowski, J. Eckstein, and I. Bozovic, Anisotropic properties of molecular beam epitaxygrown colossal magnetoresistance manganite thin films, *J. Appl. Phys*, Vol. 81, 1997, p. 4961.
[18].P K Siwach, , H K Singh and O N Srivastava, Low field magnetotransport in manganites, *J. Phys.: Condens. Matter,* 20, 273201, 2008, pp. 1-43.
[19].M. Saïb, M. Belmeguenai, L. Méchin, D. Bloyet, and S. Flament, Magnetization reversal in patterned $La_{0.67}Sr_{0.33}MnO_3$ thin films by magneto-optical Kerr imaging, *J. Appl. Phys*, Vol. 103, No. 11, 2008, p. 113905.
[20].P. Perna, L. Méchin, M. Saïb, S. Flament, Imaging the magnetization reversal of step-induced uniaxial magnetic anisotropy in vicinal epitaxial $La_{0.7}Sr_{0.3}MnO_3$ films, *New Journal of Physics,* 12, 2010, p. 103033.
[21].A. Lisauskas, J. Ba¨ck, S. I. Khartsev, and A. M. Grishin, Colossal magnetoresistive $La_{0.7}(Pb_{1-x}Sr_x)_{0.3}MnO_3$ films for bolometer and magnetic sensor applications, *J. Appl. Phys.*, Vol. 89, No. 11, 2001, p. 6961.
[22].T. McGuire and R. Potter, Anisotropic magnetoresistance in ferromagnetic 3d alloys, *IEEE Trans. Magn.,* Vol. 11, No. 4, 1975, pp. 1018– 1038.
[23].A. Jander, C. Smith, and R. Schneider, Magnetoresistive sensors for nondestructive evaluation (Invited Paper) (Proceedings Paper), in *Proceeding of the 10th SPIE International Symposium, Nondestructive Evaluation for Health Monitoring and Diagnostics, Conference 5770*, 2005.
[24].M. Díaz-Michelena, Small magnetic sensors for space applications, *Sensors*, Vol. 9, No. 4, 2009, pp. 2271–2288.
[25].M. Belmeguenai, S. Mercone, C. Adamo, L. Méchin, C. Fur, P. Monod, P. Moch, and D. G. Schlom, Temperature dependence of magnetic properties of $La_{0.7}Sr_{0.3}MnO_3$ /$SrTiO_3$ thin films on silicon substrates, *Phys. Rev. B*, Vol. 81, No. 5, 2010, p. 054410.
